Characterization of Low-Noise Quasi-Optical SIS Mixers for the Submillimeter Band

Michael C. Gaidis, *Member, IEEE*, Henry G. LeDuc, Mei Bin, David Miller, Jeffrey A. Stern, and Jonas Zmuidzinas, *Member, IEEE*

Abstract— **We report on the development of low-noise quasi-optical SIS mixers for the frequency range 400–850 GHz. The mixers utilize twin-slot antennas, two-junction tuning circuits, and Nb-trilayer junctions. Fourier-transform spectrometry has been used to verify that the frequency response of the devices is well predicted by computer simulations. The 400–850 GHz frequency band can be covered with four separate fixed-tuned mixers. We measure uncorrected double-sideband receiver noise temperatures around $5h\nu/k_B$ to 700 GHz, and better than 540 K at 808 GHz. These results are among the best reported to date for broadband heterodyne receivers.**

I. Introduction

SIS MIXERS with Nb-trilayer tunnel junctions offer excellent performance at frequencies below 800 GHz, and should perform competitively at frequencies as high as 1.4 THz [1]–[4]. Our goal was to develop a suite of low noise SIS mixers which cover frequencies from ≈400 GHz to more than 1 THz. We have demonstrated low-noise mixers at frequencies up to ≈850 GHz using devices with Nb wiring. Above 1 THz, we have made significant progress using Nb-trilayer-junction devices with normal-metal Al wiring [5]. Here we report on the lower-frequency all-Nb devices.

At frequencies below the Nb gap ($\nu < 2\Delta/h \approx 700$ GHz), existing devices perform quite well [6], but further improvements in noise temperature remain important. In addition, it is quite useful to be able to reliably predict device performance given the design parameters. This allows us to optimize the device design for a particular frequency band, and confirm that we indeed understand the physics of the device.

At frequencies above the Nb gap, RF photons can break Cooper pairs, resulting in greater signal loss and higher receiver noise temperatures. The loss is particularly important in the microstrip line used to resonate the junction capacitance. However, the actual coupling of radiation into Nb devices should still be reasonably efficient for frequencies not too far above the gap frequency—at least 30% coupling efficiency at 800 GHz, if the loss is well described by theory [7]. In addition to the RF losses, increased dispersion affects Nb microstrip circuits at frequencies near the gap. The Nb microstrip lines must, therefore, be carefully designed to ensure that the desired bandpass is achieved. We demonstrate for the first time that all-Nb SIS receivers can have substantially better performance than GaAs Schottky receivers for the astronomically important neutral atomic carbon (CI; $^3P_2 \rightarrow {}^3P_1$) and carbon monoxide (CO; $J = 7 \rightarrow 6$) transitions near 810 GHz.

Manuscript received December 6, 1995; revised March 20, 1996. This work was supported in part by Grants from NASA (NAGW-107 and NAG2-744), NASA/JPL, and a NSF PYI Grant to J. Zmuidzinas. The junction fabrication was performed at the Center for Space Microelectronics Technology, Jet Propulsion Laboratory, California Institute of Technology, and was sponsored by NASA, Office of Space Access Technology

M. C. Gaidis was with the Downs Laboratory of Physics, Jet Propulsion Laboratory 168-314, California Institute of Technology, Pasadena, CA 91109 USA. He is now with the Submillimeter-Wave Superconductive Sensor Development Group, Jet Propulsion Laboratory 168-314, California Institute of Technology, Pasadena, CA 91109 USA.

H. G. LeDuc and J. A. Stern are with the Center for Space Microelectronics Technology, Jet Propulsion Laboratory 302-231, California Institute of Technology, Pasadena, CA 91109 USA.

M. Bin, D. Miller, and J. Zmuidzinas are with the Downs Laboratory of Physics 320-47, California Institute of Technology, Pasadena, CA 91125 USA.

Publisher Item Identifier S 0018-9480(96)04717-5.

II. Receiver Configurations

Since waveguide mixers become difficult to construct at short submillimeter wavelengths, we have adopted a quasi-optical approach. Here, lenses take the place of waveguide horns, and the incoming radiation is collected by a twin-slot planar antenna on the SIS mixer substrate [8]. The quasi-optical approach offers several other advantages, such as on-chip broad-band lithographic tuning elements, straightforward scaling to yet higher frequencies, and natural adaptation to focal-plane imaging arrays.

A macroscopic view of the receiver is presented in Fig. 1 and discussed here; the microscopic description of the mixer chip follows in the next section. The local oscillators (LO) used for our measurements are compact, solid-state, tunable Gunn oscillators with varactor multipliers [9]–[11]. The signal and LO inputs are combined with 10 μm or 25 μm thick mylar beamsplitters, which couple approximately 93% or 74% of the signal power into the device, respectively, at 810 GHz. The lower LO power levels available at the higher frequencies often dictate the use of the thicker 25 μm beamsplitter. Although convenient to use, the beamsplitter can significantly increase the measured receiver noise temperature, as it replaces part of the signal with room temperature thermal noise.

The combined signal and LO travel into the dewar through a 25 μm thick mylar pressure window at room temperature, followed by a 2.5 mm thick, z-cut crystal quartz IR filter at 77 K. Both sides of this quartz disk have an additional antireflection (AR) coating which was nominally optimized for the approximate band center. (Each device uses a different IR filter, as the bandwidth of the AR coating is not sufficient to cover the entire 400–850 GHz range.) The AR coating utilizes an adhesion layer of black Xylan 1220 primer, mixed with Teflon FEP, and applied to a thickness of ≈10 μm.

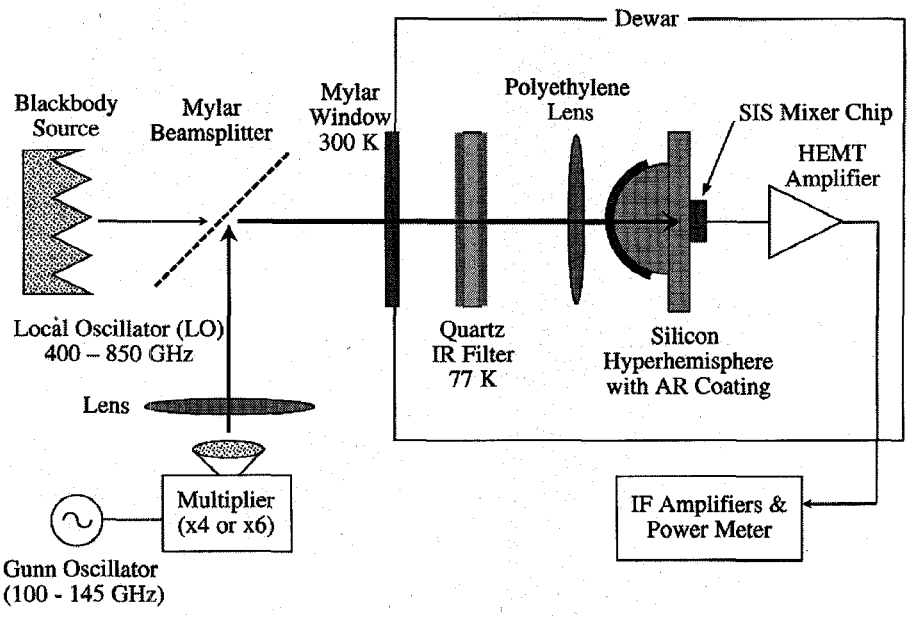

Fig. 1. Simplified receiver layout. Unless otherwise noted, elements within the dewar are mounted on a 4.2 K cold plate.

This is then covered by several layers of clear Teflon FEP to build the coating up to the requisite quarter-wavelength thickness [12]. The window and coating are quite durable and withstand repeated thermal cycling. We have not measured the IR transmission properties, but we note that for our dewar the liquid helium hold time is limited by thermal conduction via the electronic wiring, rather than by radiation through the optical port. For a filter optimized at 590 GHz, the RF loss (including reflection and absorption loss) was measured to be less than 5% at 690 GHz. This is reasonable when compared to the calculated 2.6% loss at 690 GHz.

The well-collimated ($\approx F/17$) input beam is matched to the broad pattern of the twin-slot planar antenna with a polyethylene lens and a silicon hyperhemisphere. The silicon lens is AR coated with alumina-loaded epoxy [6], [13]. The polyethylene lens and the mylar pressure window can be replaced by teflon coated quartz optics to give ≈20% overall gain in coupling efficiency at 700 GHz.

Fig. 2 presents a detailed view of the mixer block and associated circuitry. The top of Fig. 2(a) shows the magnet housing. The magnet is used to suppress Josephson effects, and consists of approximately 3600 turns of superconducting NbTi wire on a #1018 cold-rolled steel core. Steel pole pieces serve to concentrate the field at the junction to allow operation at lower magnet currents (25 mA is typical). The bottom of Fig. 2(a) shows the bias and IF circuitry and the mixer chip (at the center). As indicated in Fig. 2(b), the back side of the SIS mixer chip is glued [14] to one side of a silicon support disk, and the silicon hyperhemisphere is glued [14] to the opposite side of the disk. The SIS devices are fabricated on a 0.25 mm thick, 50 mm diameter, high-resistivity (>100 Ω-cm) silicon wafer, which is then diced into 1.2×1.5 mm individual chips. The high-resistivity (>100 Ω-cm) silicon support disk is 2.5 cm in diameter and 0.9 mm thick. The silicon hyperhemisphere consists of very high resistivity (≈4000 Ω-cm) silicon [15], diamond-machined into a 6.35 mm radius hemisphere with a 0.7 mm extension [13]. Such high resistivity silicon ensures low RF losses, but is likely not critical when operating at 4.2 K. The thicknesses of the hyperhemisphere's extension, the support disk, and the chip substrate sum to place the device at the aplanatic focus of the hyperhemisphere.

The silicon disk is clamped in the mixer block by a printed circuit board, which itself is held in place by metal clamps and screws as shown in Fig. 2(a). The circuit board is 0.6 mm thick TMM10i temperature stable microwave laminate [16], with room temperature dielectric constant 9.8 and room temperature attenuation coefficient 0.001 48 Np/cm at 10 GHz. The board's thermal expansion is isotropic, and closely matched to the gold-plated copper metallization, allowing for reliable plated-through holes and low etch shrinkage.

DC bias supply and readout leads enter from the connector on the right, and the mixer IF output is carried on a microstrip line to a SMA connector on the left. The schematic in Fig. 2(c) details the circuitry on the printed circuit board. The dc bias source resistance is adjustable by feedback to present the mixer with either a current source or a voltage source. Resistor R_{neg} is chosen at approximately 100 Ω to prevent unstable biasing due to regions of negative dynamic resistance in the SIS I–V curve. The current-sensing resistor R_{sense} is typically 10 Ω, and the IF-blocking inductors at 4.2 K add $\ll 1$ Ω series resistance. The upper 65 pF capacitor in Fig. 2(c) is attached to the IF output microstrip with silver-loaded epoxy. The lower 65 pF capacitor is attached to the ground plane via a plated-through hole with silver-loaded epoxy. The SIS mixer chip sits within a through hole at the center of the board, allowing straightforward wire-bonding of the mixer chip to the top electrodes of the two 65 pF capacitors. The chip inductors are wire-bonded to the top electrodes of the 65 pF capacitors and to the traces carrying the dc bias. The remaining chip resistors, chip capacitors, and connector pins

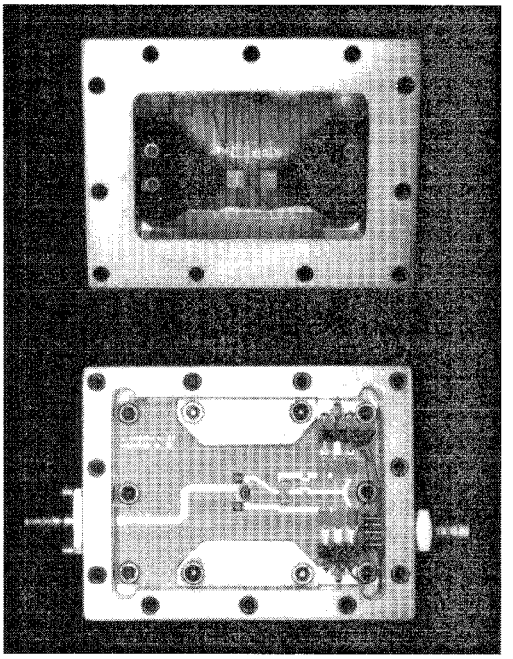

(a)

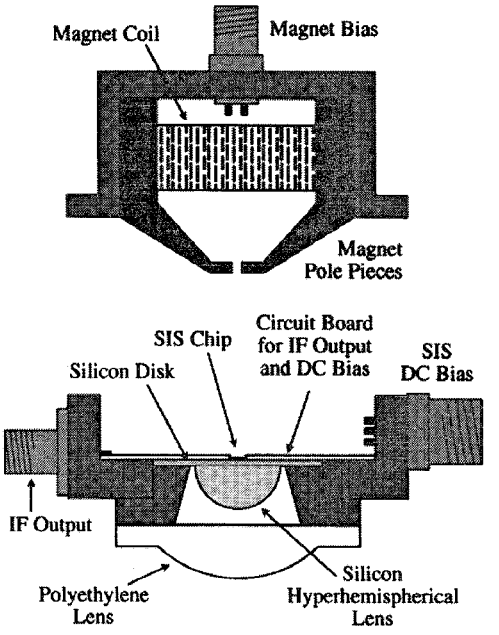

(b)

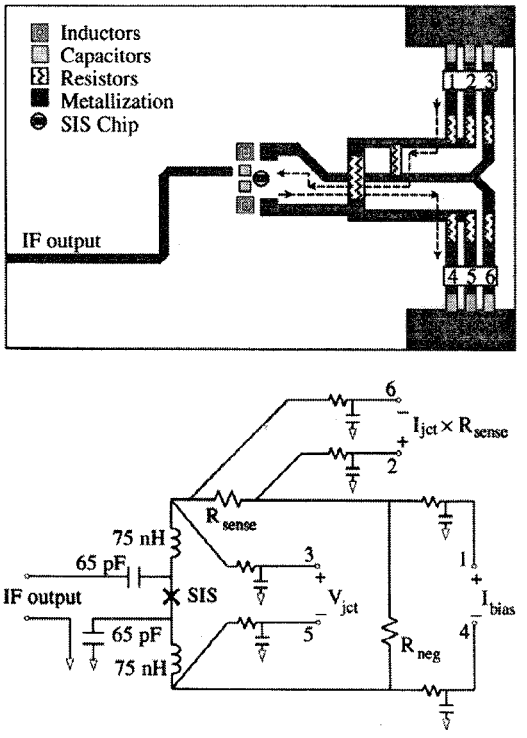

(c)

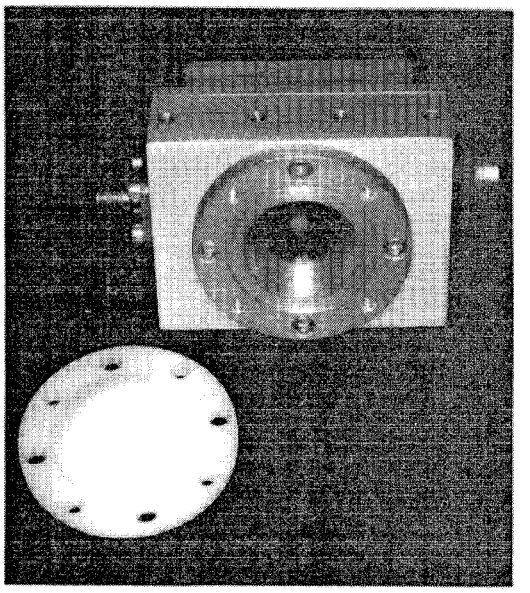

(d)

Fig. 2. Actual and schematic views of the mixer block which houses the SIS mixer chip and associated circuitry. Picture (a) shows a block disassembled to reveal the internal components. Schematic (b) provides a key to the hardware used within the block. Schematic (c) details the circuitry on the printed circuit board. Here the dc junction current bias path is denoted by a dashed line. The numbers in this schematic refer to detachable connector pins, and there is a ground plane on the reverse side of the board which connects (through screws) to the large metallized pads in the corners. The unlabeled resistors and capacitors in the circuit schematic are typically 100 Ω and 300 pF, and provide protection and filtering for the mixer. Picture (d) presents an assembled block, with the polyethylene lens removed to show the AR-coated Si hyperhemisphere. For reference, the face of the mixer block is 3.8 cm × 5.1 cm, the white polyethylene lens is 3.8 cm in diameter, and the black AR-coated Si hyperhemisphere is 1.3 cm in diameter.

are attached to the circuit board traces with either solder or silver-loaded epoxy.

The picture in Fig. 2(d) shows the assembled mixer block, with the polyethylene lens removed to reveal the silicon hyperhemispherical lens. The mixer block is attached to the cold plate with screws in the holes apparent at the top of the block. A semirigid coaxial cable connects the SMA port on the left with a HEMT low noise amplifier (LNA).

The measurements presented below were obtained using a 1.25–1.75 GHz LNA with a specified noise temperature of 3 K [17]. The LNA output is sent to room temperature amplifiers and a diode detector which measures the total power in the 500 MHz IF bandwidth.

III. Mixer Design and Fabrication

The detailed design of the twin-slot planar antenna and the two-junction SIS mixer tuning circuit has been presented elsewhere [6], [18]. Fig. 3 displays the structure representative of the mixers used in this work. In practice, the device is mounted such that the slots are horizontal with respect to Fig. 2(a). The applied magnetic field must pass beneath only a small section of microstrip in this configuration, permitting operation at lower field strengths. Shaped junctions, or a 45° rotation of the present square junctions might allow even lower applied fields, but does not seem to be an issue, as the noise temperatures appear insensitive to factors of two or three variation in the applied magnetic field. The suppression of Josephson effects in these devices is somewhat complicated by the presence of the SQUID loop and slight differences in the junction areas, but this has not been problematic.

The present mixers are quite similar to our earlier designs, except for several right-angle bends in the transformer sections. These bends allow us to better optimize the impedance match between the antenna ($\approx 30\,\Omega$) and the tunnel junctions $\approx 6\,\Omega$). We have written a computer program to simulate and optimize the RF device performance. Our circuit model includes the frequency-dependent impedance of the antennas, striplines, and tunnel junctions. The properties of the superconducting microstrip lines are calculated using our previously described method [8], which includes the frequency-dependent surface impedance of niobium as given by the Mattis–Bardeen theory in the local limit. Future improvements to the calculation will incorporate the effects of RF loss in the antenna.

The use of antisymmetrically-driven junction pairs simplifies the inductive tuning necessary to resonate the junction capacitance. The resonating inductance for each junction is simply one-half the total inductance joining the two junctions, as the antisymmetric feed creates a virtual ground at the midpoint between the two junctions [18]. Because the junctions are defined in the same lithographic step, misalignment between lithography layers will not significantly affect the tuning inductance. A misalignment will primarily produce a minor phase difference between the two slots, which then results in a slight beam tilt—approximately $2°/\mu$m—which is small compared to the beam FWHM of approximately 48°.

The relatively low antenna impedance promotes good impedance matching to even low resistance tunnel junctions. Therefore, we can design with junction areas between 1.2 μm^2 and 2.3 μm^2, which are available using JPL's all-optical-lithography junction fabrication process [8], [18]. Higher resistance submicron junctions could be fabricated using electron-beam lithography, but the processing is more difficult, and the smaller devices can be more sensitive to static discharge. In addition, large area devices are less susceptible to saturation from higher-intensity sources. One drawback of large junctions is the need for higher LO power, which scales directly with the total junction area.

The simulation program was used to generate device designs to cover the frequency range from 400–800 GHz. To allow for parameter variation, particularly in the junction areas and specific capacitance, we have included three different nominal junction sizes (1.2 μm^2, 1.7 μm^2, and 2.3 μm^2) for each tuning structure design. Each of the devices discussed below had lithographic undercut and specific capacitance such that the largest junction area devices gave the best fit to the predicted performance. Design specifications for these devices are given in Table I, and correlate with the diagram in Fig. 3. The devices all utilized a 2.5 μm length of microstrip (with width equal to the inductor width) to connect the last transformer section with the inductor section. The overall capacitance of these devices allows a broadband IF output (>4 GHz bandwidth).

IV. Receiver Performance

A. Fourier-Transform Spectroscopy

The receiver response as a function of frequency was measured with an FTS system (built in-house) using the mixer as a direct detector [19]. The FTS operates in a purged nitrogen atmosphere, with a 50 μm mylar beamsplitter and a source consisting of a variable 300–1200 K resistively-heated wire [20] chopped against a 77 K eccosorb load. Generally, the (unheated) 300 K source gives sufficient signal to allow scanning with 3.6 GHz resolution and 3.7 THz bandwidth in less than 30 minutes. Resolution of $\approx$100 MHz has been demonstrated with this FTS, and allows separation of the sidebands when the detector is operated in heterodyne mode (see below).

Although we cannot yet reliably measure the *absolute* response using the FTS, the *shape* of the relative response versus frequency is quite reliable and useful. The *absolute* response of different devices is best compared by performing heterodyne measurements. As the RF junction impedances in heterodyne and direct operation typically differ by less than 10%, the direct FTS measurements can be expected to give a relatively accurate indication of the device frequency dependence in heterodyne mode [21], [22]. We have found that the variation of the noise temperature with frequency correlates well with the response measured on the FTS, so that we can rely heavily on FTS data to select useful devices from a given fabrication run.

Fig. 4 illustrates the accuracy with which we can predict mixer response at present. The simulation curves give the fraction of the power received by the antenna which is dissipated in the junctions. The vertical scaling of the FTS data is adjusted to give the best match to the simulation. This is considered valid, as coupling differences between FTS runs should be frequency-independent.

In general, the agreement between simulation and experiment is quite good, given the nonidealities present in the measurement: strong water absorption lines at 557 and 752 GHz, and Fabry–Perot resonances from the quartz IR filter spaced approximately 50 GHz apart. These resonances are

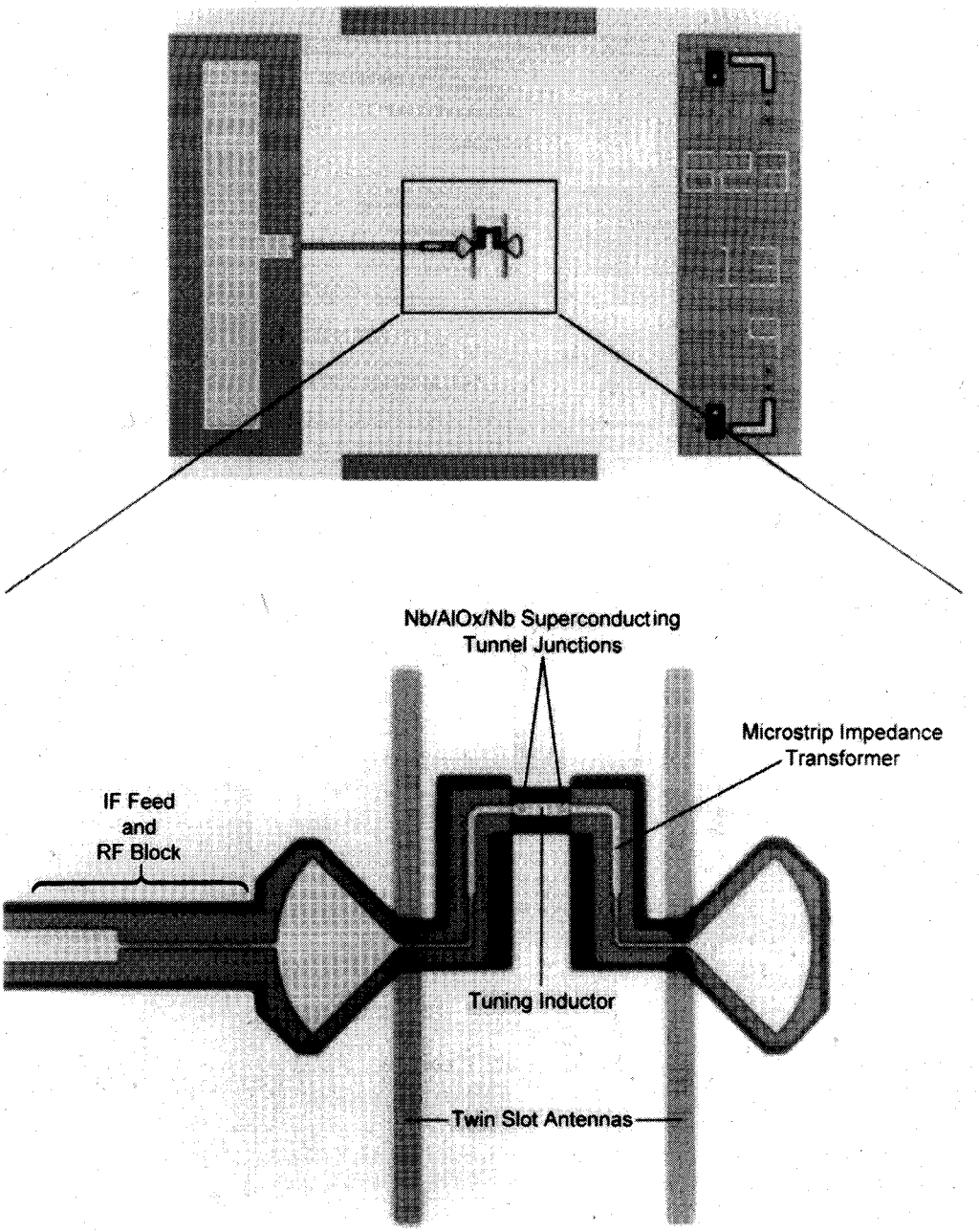

Fig. 3. Twin-slot antenna, two-junction SIS mixer design (top view). The upper portion of the figure shows the entire 1.2 mm × 1.5 mm mixer chip. Wire bonds make contact to the ground plane and to the large pad on the left. The lower portion of the figure details the device. The two vertical slots in the ground plane form the antenna, which is sensitive to horizontal polarization. The radial stubs couple RF current into the transformer sections and then to the tunnel junctions. The two tunnel junctions connect the ground plane to the microstrip line, and are linked by a microstrip line which serves as an inductor to tune the junction capacitances. SiO forms the microstrip insulator, 400 nm thick at the radial stubs and impedance transformers, and 200 nm thick at the tuning inductor. The 1.5 GHz IF is coupled out using a long section of coplanar waveguide (CPW) that is attached to the RF choke on the left.

particularly noticeable in Fig. 4(d), where the "bandpass" of the AR-coating on the quartz IR filter does not extend below about 700 GHz. Only two corrections have been made to the FTS data: for the optical efficiency of the mylar beamsplitter within the FTS, and for the quantum responsivity of the detector, which scales as $1/\nu$.

The most significant deviations from theory occur in device 43 near 700 GHz, in device 53 near 600 GHz, and in device 73 above 800 GHz. The reduced response apparent in the FTS data or device 43 near 700 GHz is due to a $\approx$91.5% decrease in the antenna main-beam efficiency, which is not incorporated into the simulation. We presently do not understand the discrepancy in device 53. The deviation in device 73 above 800 GHz may be due in part to antenna losses, decreased main-beam efficiency, and a larger-than-expected surface impedance loss in Nb above the gap frequency.

More than 20 different devices have been tested in this manner to date, and all agree with the simulations to a degree represented by the graphs in Fig. 4, thus indicating that our simulation method is reasonably reliable. For a given

TABLE I
DESIGN PARAMETERS FOR REPRESENTATIVE DEVICES

Parameter	Device 43	Device 53	Device 63	Device 73
Optimization Bandwidth (GHz)	400 - 500	500 - 600	600 - 700	700 - 800
Nb Ground Plane, Microstrip Thickness (nm)	200	200	200	200
90° Radial Stub Radius (μm)	36	36	36	36
Antenna Slot Size (μm^2)	222 × 11	182 × 9.1	154 × 7.7	133 × 6.7
Slot Spacing (μm)	110	91	77	67
1st Transformer Section ($w \times l$, μm^2)	2.0 × 51.9	2.0 × 45.9	2.0 × 37.7	5.8 × 15.0
2nd Transformer Section ($w \times l$, μm^2)	4.6 × 62.3	4.7 × 50.7	4.5 × 41.1	3.3 × 15.0
SiO Thickness: Transformer Microstrip (nm)	400	400	400	400
SiO Thickness: Inductor Microstrip (nm)	200	200	200	200
Nominal Junction Area (μm^2)	1.5 × 1.5	1.5 × 1.5	1.5 × 1.5	1.5 × 1.5
Corrected Junction Area (μm^2)	1.3 × 1.3	1.3 × 1.3	1.3 × 1.3	1.3 × 1.3
Inferred Jct. Specific Capacitance (fF/μm^2)	80	85	85	85
Junction Resistance-Area Product (Ω μm^2)	19.6	18.0	19.9	19.6
Inductor (Between Jct. Centers; $w \times l$, μm^2)	5.0 × 23.5	5.0 × 14.9	5.0 × 9.8	5.0 × 6.9

fabrication run, the junction capacitance is the only significant variable parameter. When this is fixed by FTS data from one device, the FTS data from remaining devices on the same wafer will closely match the simulations with no fittable parameters (other than the arbitrary amplitude scaling). Recent device batches have consistently yielded specific capacitances of 85 ± 5 fF/μm^2. This is determined from FTS measurements of the device bandpass, as compared with simulations (below the Nb gap), and is adjusted for junction area variations through the use of test die on the device wafer. For the devices presented in Fig. 4, the undercut in the junction dimensions was measured to be $\approx$200 nm. The uncertainty and variation in the junction areas limits the accuracy with which we can determine the junction specific capacitance. The (minor) observed variations in junction resistance have only a small effect on the overall bandwidth.

B. Heterodyne Measurements

We have measured the noise temperatures of several devices, including those in Fig. 4, using the Y-factor method. Our noise temperatures are referred to the input of the beamsplitter; unless otherwise noted, *no corrections have been made for beamsplitter or other optical losses*. Fig. 5 shows the dc current-voltage characteristics of device 73. The pumped (839 GHz) and unpumped I–Vs are shown for a bath temperature of 2.7 K. The second Shapiro step is visible at $\approx$3.5 mV, and the photon step from the nonlinearity at $V = -2\Delta/e \approx -2.9$ mV appears at $V \approx +0.6$ mV, as expected from the 839 GHz LO input ($h\nu/e \approx 3.5$ mV). Also shown in Fig. 5 are the total IF output power in a 500 MHz bandwidth when room temperature and 77 K absorbers are placed at the receiver input. The curves are relatively smooth (particularly near the first Shapiro step), indicating good suppression of Josephson noise. With no mechanical tuning elements—simply adjustment of the junction dc bias, magnetic field, and LO power—this device gives a DSB receiver noise temperature of 722 K at the 839 GHz LO frequency.

Fig. 6 displays receiver noise temperatures as a function of frequency for several of our best devices at a bath temperature of 4.2 K. The high-frequency (#73) device was also tested at a pumped-LHe temperature of 2.7 K, with resulting noise temperatures displayed with open markers. Upon cooling to 2.7 K, the noise decreases by more than 100 K over most of the band, in part due to the reduced dark current and its shot noise. (The dark current here typically represents $\approx$40% of the total LO-pumped bias current at 4.2 K.)

Particularly at the higher frequencies, the receiver noise temperatures are adversely affected by the relatively low output power of our LO chains ($<100\,\mu$W typically). The situation is further degraded by our relatively large junctions, which require $\approx$300 nW of LO at 750 GHz [21]. This could be reduced to $\approx$50 nW through the use of existing submicron junction technology. The use of thicker beamsplitters to couple in more LO power does not improve the receiver noise temperature, as a greater portion of the signal is reflected away from the mixer, and replaced by 300 K radiation. Device 73 would offer significantly lower noise temperatures if a stronger LO source and a thinner beamsplitter were employed. If we correct for beamsplitter losses, the 839 GHz, 4.2 K receiver noise temperature drops from 1100 K to $\approx$800 K. The anomalously low noise temperature of device 73 at 4.2 K and 761 GHz is the result of a more powerful LO. At this frequency, we were able to use a far-infrared laser LO source, which produces a good deal more power than our standard LO chain. A thinner beamsplitter was employed ($\approx 6\,\mu$m thick mylar) to improve the signal coupling efficiency.

To our knowledge, the (uncorrected) results presented in Fig. 6 are the best, or near the best for any broadband heterodyne receiver. At frequencies below the Nb gap, optical losses are likely to be the dominant contribution to the receiver noise temperature. Although the noise temperatures increase with frequency dramatically above the gap due to increased RF losses in the Nb, the 800 GHz results are particularly impressive if compared with the nearest competitor—GaAs Schottky corner-cube receivers at 1500 K (*after* correcting for the $\approx$50% corner-reflector antenna efficiency) [23].

We have also, for the first time, measured the FTS heterodyne response of a SIS mixer at sufficiently high resolution to resolve the LO and sideband frequencies. This measurement verifies that our devices do in fact perform as mixers. Fig. 7 shows the FTS response of device 73, but in heterodyne

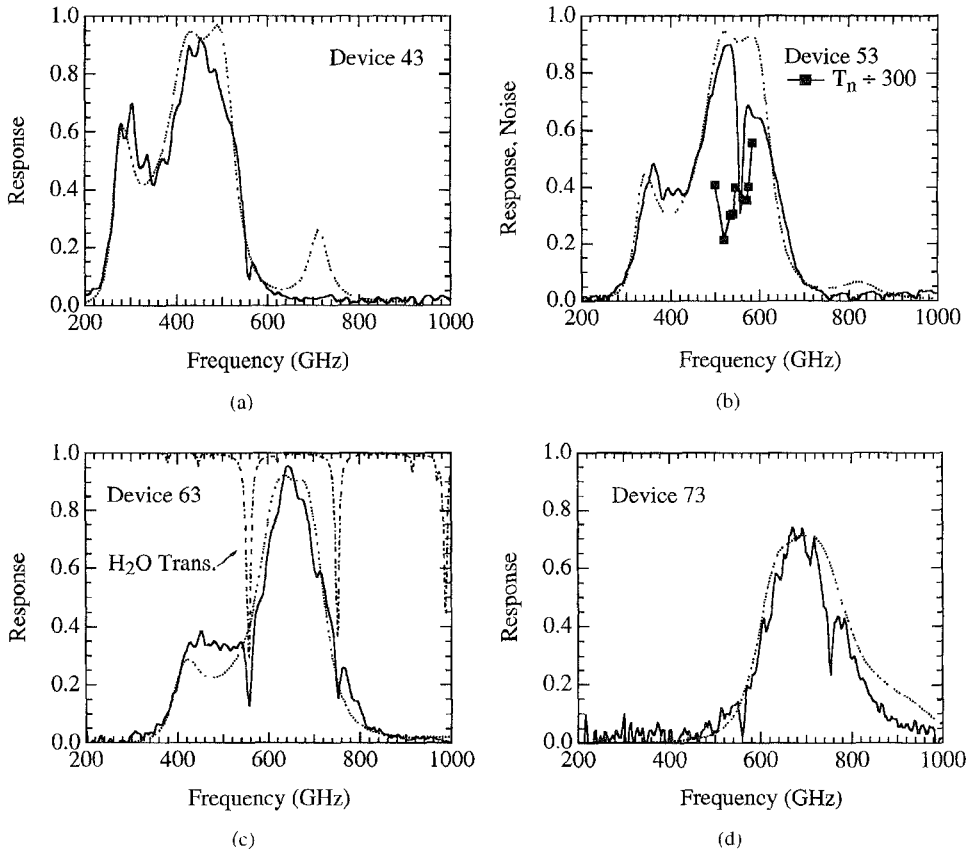

Fig. 4. FTS measured response (solid lines) versus mixer simulation (dashed lines) for the four devices spanning the 400–850 GHz band. Graph (b) includes (uncorrected) DSB noise temperatures for comparison with the FTS response. Graph (c) includes a curve representative of submillimeter transmission through the residual water vapor in the FTS. The device labels on the graphs correspond to the column headings of Table I.

mode, with a 742 GHz local oscillator illuminating the device during the FTS measurement. The spectrum [Fig. 7(b)] clearly shows significant response only near the LO frequency. The IF bandwidth and double-sideband operation are evident from the inset. The negative-going portion of the signal results from ringing in the Fourier-transforming procedure. Presumably the upper sideband peak is weaker than the lower sideband peak because of absorption near the 752 GHz water line. The FTS interferogram [Fig. 7(a)] shows the high frequency oscillations characteristic of the 742 GHz LO (see inset), modulated by the 3 GHz sideband separation and the 500 MHz IF bandwidth.

V. Applications

We have been able to take advantage of the low 800 GHz receiver noise temperatures during observing runs aboard NASA's Kuiper Airborne Observatory KAO) in June 1995. We detected the CI ($^3P_2 \rightarrow {}^3P_1$) and CO ($J = 7 \rightarrow 6$) transitions in the M17 HII region/molecular cloud complex. Fig. 8 shows the data obtained with the double-sideband receiver, with an LO frequency of 807.8 GHz, and a 1–2 GHz IF band. The CI line lies in the upper sideband, at 809.3 GHz, while the CO line is found in the lower (image) sideband at 806.7 GHz. The nonzero baseline is indicative of dust continuum emission. Unfortunately, we were not able to use our best device at this frequency for these observations. Nonetheless, we achieved a double-sideband system noise temperature (including telescope coupling, spillover, and atmospheric losses) of better than 2000 K.

VI. Conclusion and Outlook

We have demonstrated low-noise SIS receivers with *predictable* performance at frequencies from ≈400 GHz to above 800 GHz. Our device simulation program can accurately predict the experimentally observed performance, giving us the ability to reliably design broadband, high sensitivity devices over our frequency range of interest. Fourier-transform spectroscopy has been used as a powerful tool for testing our predictions, and for selecting useful devices and optical configurations. We have also used heterodyne FTS measurements to verify the mixing behavior of our SIS devices well into the submillimeter region.

Our SIS receivers are the first to demonstrate substantially better performance than GaAs Schottky receivers for the astrophysically important CI and CO transitions near 810 GHz. Our quasi-optical devices are fully competitive with existing waveguide mixers at frequencies as low as 400 GHz. The simplicity and flexibility of the quasi-optical approach further increase the desirability of these devices at higher frequencies and for imaging arrays.

Future work will concentrate on understanding the apparently excessive losses above 800 GHz, and will attempt to minimize this problem through the use of lower-loss wiring

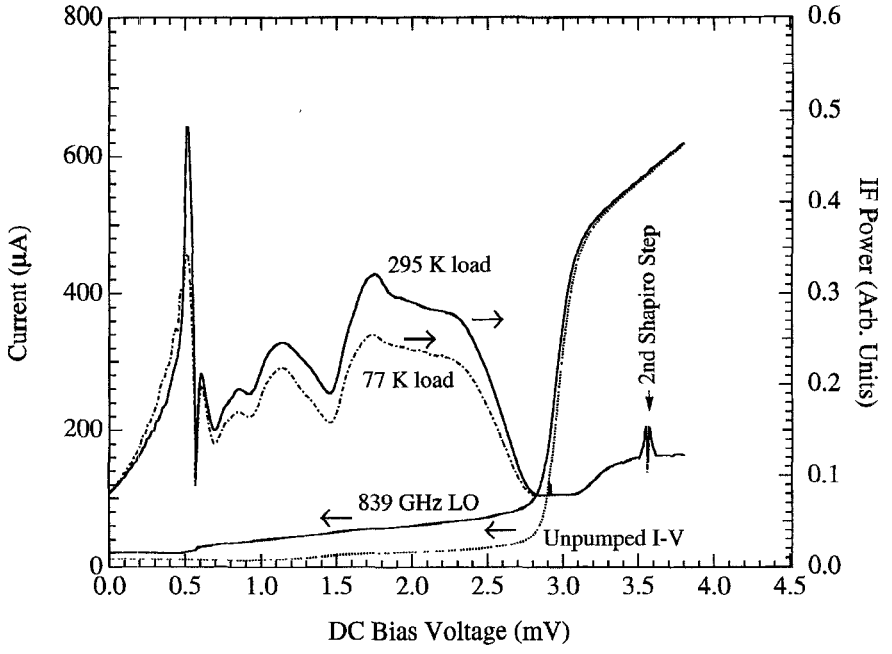

Fig. 5. Current versus voltage and IF power versus voltage for device 73 at 2.7 K. The LO frequency is 839 GHz, and the DSB receiver noise temperature is 722 K.

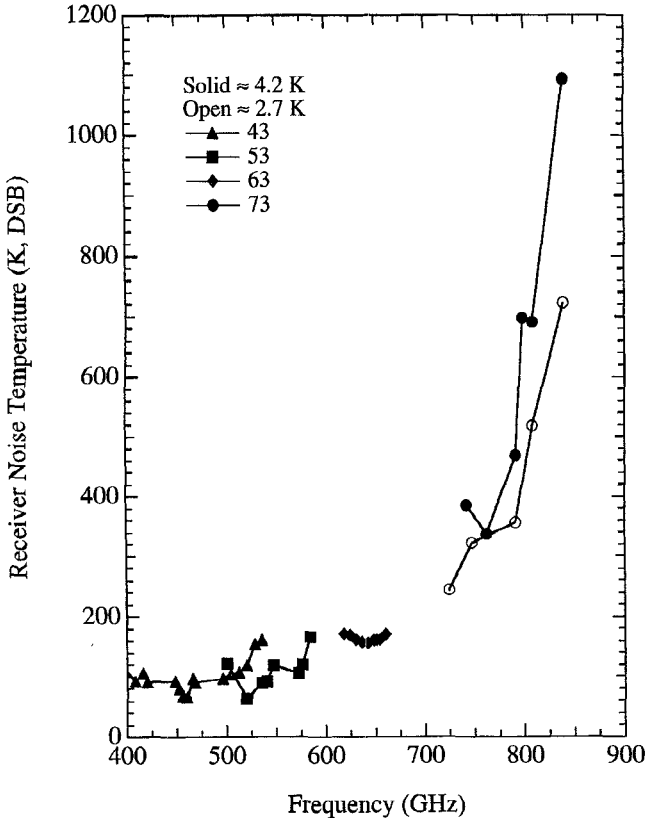

Fig. 6. Uncorrected DSB noise temperatures of the devices described in Table I. Note the superconducting gap $2\Delta/h$ is ≈700 GHz for our Nb films. Due to RF loss in the Nb, noise temperatures exhibit a sharp increase above this frequency.

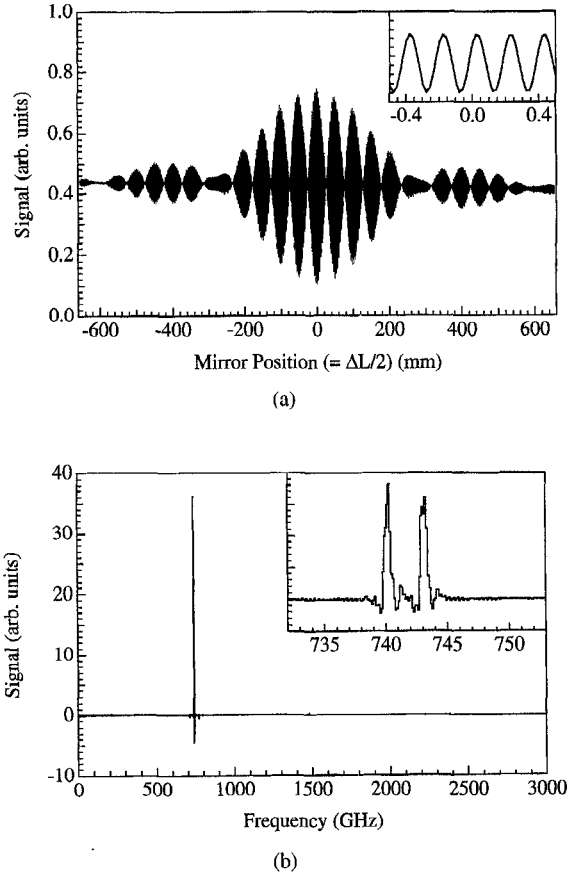

Fig. 7. Heterodyne FTS interferogram (a), Fourier-transformed to give the spectrum (b) for device 73 operated as a mixer. A 742 GHz LO illuminated the device during the FTS scan.

materials such as Al and NbN. Initial results with quasi-optical twin-slot double-junction devices using normal-metal Al wiring are quite encouraging, giving a noise temperature of 840 K at 1042 GHz [5]. With further optimization of

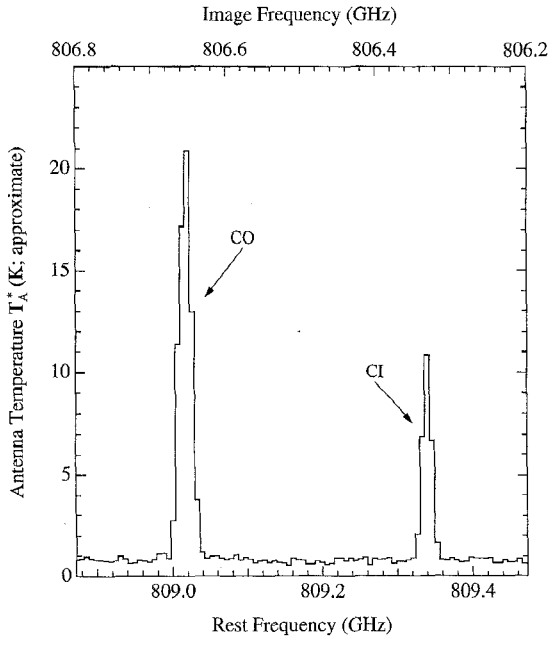

Fig. 8. Observed emission from the CI ($^3P_2 \rightarrow {}^3P_1$) and CO $J = 7 \rightarrow 6$) transitions in M17.

the optical configuration, this device noise temperature could improve significantly.

ACKNOWLEDGMENT

The authors would like to thank N. Erickson for the use of his 800-GHz multiplier chain, and G. Blake and P. Stockman for help with the FIR laser. We also wish to acknowledge advice and laboratory contributions from T. Büttgenbach, A. Clapp, J. Kooi, T. Phillips, P. Schaeffer, R. Schoelkopf, N. G. Ugras, and J. Ward.

REFERENCES

[1] G. DeLange, C. E. Honingh, J. J. Kuipers, H. H. A. Schaeffer, R. A. Panhuyzen, T. M. Klapwijk, H. Van de Stadt, and M. M. W. M. de Graauw, "Heterodyne mixing with Nb tunnel junctions above the gap frequency," *Appl. Phys. Lett.*, vol. 64, pp. 3039–3041, 1994.

[2] D. Winkler and T. Claeson, "High frequency limits of superconducting tunnel junction mixers," *J. Appl. Phys.*, vol. 62, pp. 4482–4498, 1987.

[3] M. J. Wengler and D. P. Woody, "Quantum noise in heterodyne detection," *IEEE J. Quantum Electron.*, vol. 23, pp. 613–622, 1987.

[4] W. C. Danchi and E. C. Sutton, "Frequency dependence of quasiparticle mixers," *J. Appl. Phys.*, vol. 60, pp. 3967–3977, 1986.

[5] M. Bin, M. C. Gaidis, J. Zmuidzinas, T. G. Phillips, and H. G. LeDuc, "Low-noise 1 THz niobium superconducting tunnel junction mixer with a normal metal tuning circuit," *Appl. Phys. Lett.*, vol. 68, pp. 1714–1716, Mar. 18, 1996.

[6] J. Zmuidzinas, N. G. Ugras, D. Miller, M. Gaidis, H. G. LeDuc, and J. A. Stern, "Low-noise slot antenna SIS mixers," *IEEE Trans. Appl. Superconduct.*, vol. 5, pp. 3053–3056, 1995.

[7] R. Pöpel, "Electromagnetic properties of superconductors," in *Superconducting Quantum Electronics*, V. Kose, Ed. Berlin: Springer-Verlag, 1989, pp. 44–78.

[8] J. Zmuidzinas and H. G. LeDuc, "Quasi-optical slot antenna SIS mixers," *IEEE Trans. Microwave Theory Tech.*, vol. 40, pp. 1797–1804, 1992.

[9] J. E. Carlstrom, R. L. Plambeck, and D. D. Thornton, "A continuously tunable 65–115 GHz Gunn oscillator," *IEEE Trans. Microwave Theory Tech.*, vol. 33, pp. 610–619, 1985.

[10] N. R. Erickson and J. Tuovinen, "A waveguide tripler for 720–880 GHz," in *Proc. Sixth Int. Symp. Space Terahertz Tech.*, Caltech, Pasadena, CA, Mar. 21–23, 1995, pp. 191–198.

[11] R. Zimmerman, T. Rose, T. W. Crowe, and T. W. Grein, "An all solid-state 1 THz radiometer for space applications," in *Proc. Sixth Int. Symp. Space Terahertz Tech.*, Caltech, Pasadena, CA, Mar. 21–23, 1995, pp. 13–27.

[12] Thermech Engineering Corp., 1773 W. Lincoln Ave., Bldg. K, Anaheim, CA 92801.

[13] Janos Technology, Inc., HCR #33, Box 25, Route 35, Townshend, VT 05353-7702.

[14] Litetak 3761 UV-curing adhesive, by Loctite Corp., Hartford, CT 06106.

[15] Topsil US, 25 Burlington Mall Rd., Suite 300, Burlington, MA 01803.

[16] Rogers Corporation, Microwave Circuit Materials Division, 100 S. Roosevelt Ave., Chandler, AZ 85226.

[17] Berkshire Technologies, Inc., 5427 Telegraph Ave., Suite B2, Oakland, CA 94609; model L-1.5-30HI.

[18] J. Zmuidzinas, H. G. LeDuc, J. A. Stern, and S. R. Cypher, "Two-junction tuning circuits for submillimeter SIS mixers," *IEEE Trans. Microwave Theory Tech.*, vol. 42, pp. 698–706, 1994.

[19] Q. Hu, C. A. Mears, P. L. Richards, and F. L. Lloyd, "Measurement of integrated tuning elements for SIS mixes with a Fourier transform spectrometer," *Int. J. IR MM Waves*, vol. 9, pp. 303–320, 1988.

[20] Perkin-Elmer Corp., 7421 Orangewood Ave., Garden Grove, CA 92641, part number 17-1079.

[21] J. R. Tucker and M. J. Feldman, "Quantum detection at millimeter wavelengths," *Rev. Mod. Phys.*, vol. 57, pp. 1055–1113, 1985.

[22] T. H. Büttgenbach, H. G. LeDuc, P. D. Maker, and T. G. Phillips, "A fixed tuned broadband matching structure for submillimeter SIS receivers," *IEEE Trans. Appl. Superconduct.*, vol. 2, pp. 165–175, 1992.

[23] A. I. Harris, J. Stutzki, U. U. Graf, and R. Genzel, "Measured mixer noise temperature and conversion loss of a cryogenic Schottky diode mixer near 800 GHz," *Int. J. Infrared Millimeter Waves*, vol. 10, pp. 1371–1376, 1989.

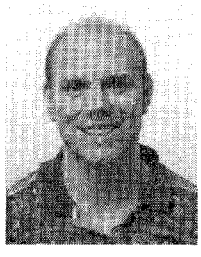

Michael C. Gaidis (M'88) was born in Madison, WI, on March 10, 1967. He received the B.S. degrees in physics and electrical engineering, the M.S. degree in electrical engineering from the Massachusetts Institute of Technology in 1989, and the Ph.D. degree in applied physics from Yale University in 1994. His Ph.D. thesis involved the development of superconducting tunnel junctions as single-photon x-ray detectors.

Since June 1994, he has been a Postdoctoral Research Fellow at the California Institute of Technology. The main thrust of his research at Caltech has been the development of SIS receivers for submillimeter astronomy. His research interests include useful applications of superconducting devices and their underlying physical mechanisms.

Henry G. LeDuc was born in Butte, MT on March 8, 1955. He received the B.S. degree in physics from Montana State Univ., Bozeman, MT in 1977, and the Ph.D. degree in physics from the University of California, Davis, in 1983. His thesis work involved far-infrared spectroscopy of solid state ionic conductors.

He is a group leader at the California Institute of Technology's Jet Propulsion Laboratory. His group develops SIS tunnel junctions for heterodyne receivers.

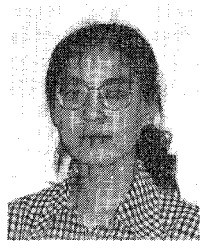

Mei Bin received the B.S. degree in physics from Tsinghua University, Beijing, China, in 1987. She is now finishing her Ph.D. study at the California Institute of Technology, Pasadena, CA. Her thesis work involves FTS studies of SIS detectors and the development of THz Nb-based SIS mixers using normal-metal tuning circuits.

Her research interests are in the area of superconducting devices and their applications to microwave technology.

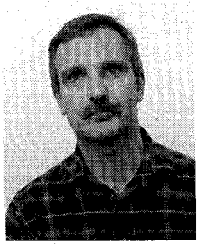

David Miller was born in Portsmith, VA on May 1, 1959. He received the B.S. degree in electrical engineering from the California State Polytechnic Univ. at Pomona in 1990, and is presently enrolled in the M.S.E.E. program at this university.

Currently, he is an Associate Engineer in the submillimeter group at the California Institute of Technology, Pasadena, CA. His primary responsibilities have involved the development of quasi-optical SIS receivers for submillimeter astronomy from the Kuiper Airborne Observatory and the Caltech Submillimeter Observatory. His research interests include characterization and measurements of antenna patterns of twin-slot SIS receivers and their associated optics.

Jeffrey A. Stern was born in Baltimore, MD, on September 16, 1961. He received the B.S. degree in physics from Rensselaer Polytechnic Institute in 1983, and the Ph.D. degree in applied physics from the California Institute of Technology in 1991. His Ph.D. thesis described the fabrication and testing of 200 GHz NbN/MgO/NbN SIS mixers.

He is with the Jet Propulsion Laboratory, developing niobium and niobium-nitride based SIS tunnel junctions for use as mixers in the millimeter and submillimeter wavelength band.

Jonas Zmuidzinas (M'91) was born in Duarte, CA, on September 8, 1960. He received the B.S. degree in physics from the California Institute of Technology in 1981, and the Ph.D. degree in physics from the University of California, Berkeley, in 1987. His Ph.D. thesis described the development of a laser heterodyne receiver for airborne astronomy in the far-infrared (800–2000 GHz).

From 1988 to 1989, he was a postdoctoral fellow at the University of Illinois, where he worked on the design and fabrication of SIS mixers. He is currently an Associate Professor of Physics at the California Institute of Technology. His research interests are in the areas of high-frequency superconducting devices and their application to submillimeter astronomy.